A Numerical Procedure for the Preliminary Design of a ORC Power Plants with Positive Displacement Expanders

T. DONATEO, A. FAZIO
Department of Engineering for Innovation
University of Salento
Via per Arnesano, 73100
ITALY
teresa.donateo@unisalento.it

Abstract: - Organic Rankine Cycle power plants use organic, high molecular mass fluids to allow heat recovery from lower temperature sources such as industrial waste heat, geothermal heat, solar etc. The expansion process is usually carried out by axial or radial turbines. However, when the available thermal power is less than 1000 kW, the usage of positive-displacement expander becomes more suitable. In the present investigation, only Scroll expanders have been taken into account. A model has been developed to evaluate the efficiency and the performance of both the overall ORC power plant and the positive displacement expander. A multi-objective genetic algorithm is used for the optimization of the power plant to select the main design parameter of the plant like evaporator pressure, overheating, thermal recovering, mass flow rate etc. The power plant has been optimized based on the local radiating solar energy distribution obtained by statistical data on the local site (Lecce - Italy) during the year 2007. Several alternative refrigerants, such as R123, R245fa and R134a have been taken into account.

Key-Words: - ORC, positive displacement expander, multi-objective optimization , solar energy.

1 Introduction

Power plants using a high molecular fluid to perform a Rankine cycle are named ORC (Organic Rankine Cycle) power plants ([1]-[4]). The most common ORC configuration consists essentially of a heat recovery vapor generator, a power turbine, a condenser and a circulating pump. The corresponding cycle is show in Fig. 1. Note that at the exit of the expander, the organic fluid can be in the state of over-heated vapor. Thus, a heat exchanger can be added to the standard configuration of an elementary Rankine power plant to transfer heat from the hotter working fluid to the colder liquid that exit the pump (regeneration).

Working fluids are chosen so that they can be subjected to the evaporation phase and (if any) over-heating at a low temperature, thus enabling the recovery of heat from sources at low temperature, and with limited and discontinuous available power (solar, biomass, geothermal, waste heat in general). In addition to this requirement, the working fluids must present an acceptable pressure in the processes of heat exchange, low freezing point, high stability to temperature changes, high heat of vaporization, high density and low environmental impact. Moreover, they must be available at low cost, non-flammable, non-corrosive and non-toxic in order to ensure safety. ASHRAE [5] offers a list of potential working fluid for ORC plant. The thermodynamic properties of such fluids can be evaluated by using the REFPROP (Reference Fluid Thermodynamic and Transport Properties Database) a software developed by the National Institute of Standards and Technology [6].

The use of energy sources with different characteristics in terms of available power and maximum temperature reached in the cycle requires, in fact, to tie the design parameters of the system (vaporization pressure, amount of overheating, condensing pressure, etc.) to the thermodynamic characteristics of the working fluid in order to achieve the best efficiency.

Several studies can be found in literature about the choice of the working fluid once the design parameters of the power plant have been defined. Among them, Wang and Zhao [7] analyze the use of binary zeotropic mixtures of R152a and R245fa as working fluids of the solar ORC in a direct vapor generation configuration.

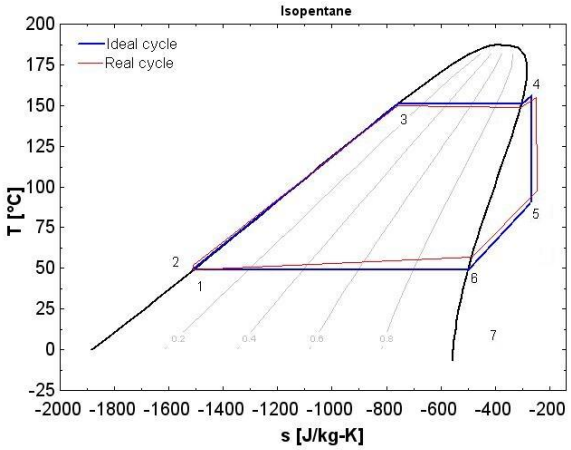

Fig. 1 Working cycle of an ORC power plant using Isopentane

Kosmadakis et al. [8]present a working fluid selection study for the top cycle of a double cascade solar ORC. Tchanche et al. [9] followed a similar approach using first and second laws of thermodynamics to carry out an investigation of the performance of low-temperature solar ORC cycles with twenty working fluids. Wolpert and Riffat [10] make the study of a low-temperature (<100 °C) solar ORC design for electricity generation by optimizing of the overall solar power cycle efficiency using four different working fluids. Delgado-Torres et al. [11], propose the optimization of the solar power cycle through the maximization of the net overall efficiency of the solar power cycle by a selection of a set of operating fluids. The research described in this paper differs from these works in that the choice of the working fluid is performed simultaneously with the design parameters of the plant as well as to the specification of the expander. All the design parameters, in fact, have been incorporated in a single optimization process, which allows, for a fixed thermal power, the maximum efficiency to be obtained.

In an ORC power plant, the expander is the most critical component since the performance and efficiency of the whole plant depend greatly from those of the machine that performs the expansion process. The most widespread ORC systems involve the use of turbines, which compared to conventional Rankine have to work with lower flow rate. They are often designed with the radial configuration and are run at lower speed of rotation with a consequent reduction of mechanical stress.

Other advantages of ORC with respect to traditional Rankine power plant include:

- The possibility to run the turbine at lower speed (i.e. direct drive of the electric generator without reduction gear, low mechanical stress of the turbine, thanks to the lower peripheral speed);
- No erosion of the turbine blades thanks to the absence of moisture in the vapor nozzles;
- A longer operational life of the machine due to the characteristics of the working fluid that, unlike steam, is non-eroding and non-corroding for valve seats, tubing and turbine blades;
- Simple start-stop procedures;
- quiet operation;
- minimum maintenance;
- good partial load performance;
- The condenser can be air cooled while keeping relative high cycle efficiency, thus avoiding the necessity of water treatment system as in steam plants.

Many studies in the literature have shown that positive displacement machines are advantageous compared to turbo machines for low-temperature applications [12]- [16] especially when thermal power is available at very low temperature and fluid flow rates are small. Positive displacement expanders for this kind of application are usually obtained from Scroll or screw compressors with some modification to be used as power generating machines. For the choice of the expander typology, the range of thermal power reported in Fig. 2 can be useful [13].

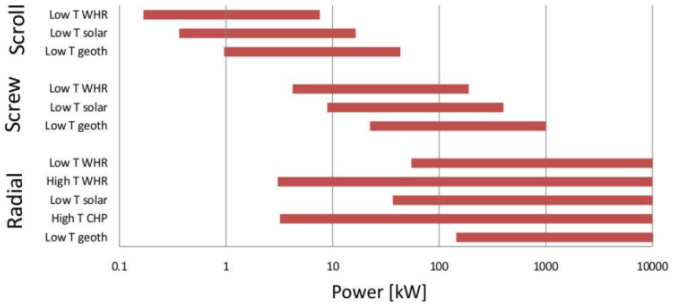

Fig. 2 Choice of the expander configuration versus thermal power (adapted from [13])

Note that, if thermal power is higher than 5kW and lower than 50kW, Scroll expanders, screw expanders and radial turbines can all be considered while at higher values of power (50-1000kW) only screw expanders and radial turbines are suitable. In the proposed methodology, the selection of the expanders is performed together with the other design and control parameters of the power plants. However, the expander model has been validated only for Scroll expander. Thus, only this kind of expander will be taken into account in the test case described in the present investigation.

2 Design procedure

The design of the ORC power plant begins from the rated values of power and temperature of thermal source and by the availability of cooling medium. Then, the following design parameters can be chosen: type of expander, expander specification, organic fluid, evaporation pressure, overheating, regeneration and condenser pressure. These parameters should be accurately chosen to maximize the overall efficiency of the power plant. In the present investigation, an automated procedure is proposed for the design of the power plant. It consists of the following steps:

A. Specification of the thermal source;
B. Choice of the working fluid;
C. Calculation of thermodynamic properties and flow rate;
D. Detailed modeling of the expander;
E. Calculation of net power and efficiency;
F. Optimization with genetic algorithms.

The procedure has been implemented in Matlab. It will be applied to a small size solar power plant using scroll expander. The power plant is simulated as a sequence of logic blocks, each describing a particular component with a degree of detail that depends on the importance of that component on the overall performance of the power plant (see Fig. 3). The thermodynamic state of the organic fluid that performs the cycle is represented with a number according to the following sequence of thermodynamic processes:

1-2: a pump compresses the liquid organic fluid;
2-3: Liquid fluid is pre-heated in the regenerator block;
3-4: Liquid fluid goes through the vapor generator where it is heated up to the evaporation temperature, is evaporated and over-heated until reaching the maximum temperature that can be guaranteed by the thermal power;
4-5: over-heated vapor expands in the power-generating machine producing mechanical work:
5-6: organic fluid at the exit of the expander is still in the state of over-heated vapor and can transfer heat to the regenerator block;
6-7 organic fluid enters the condenser where it is condensed with the use of an appropriate cooling fluid.

2.1 STEP A: Specification of the thermal source

A solar ORC power plant has been considered in the present investigation. The rated values of power and temperature of the thermal source have been set according to the information about the availability of solar energy in Lecce during year 2007 contained in the TRNSYS [18] database. The database gives the availability of solar power in each hour during year 2007 (see Fig. 4). The data have been worked out to obtain the frequency distribution between 0.3 and 200 kW (Fig. 5). In this range of power, both positive displacement and turbo machine can be used as expander as illustrated in Figure 2. Since this first application of the method only includes Scroll expander, the maximum solar power considered will be 50kW.

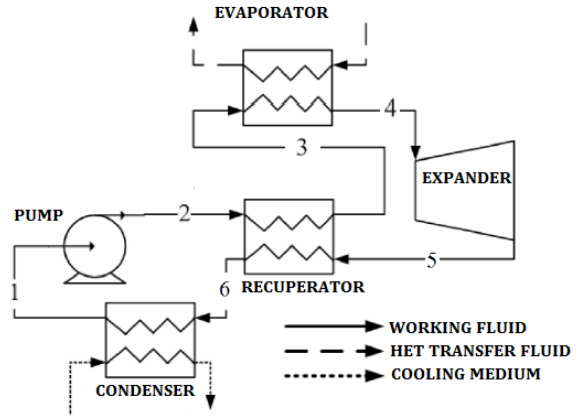

Fig. 3 Components of the ORC power plant included in the model

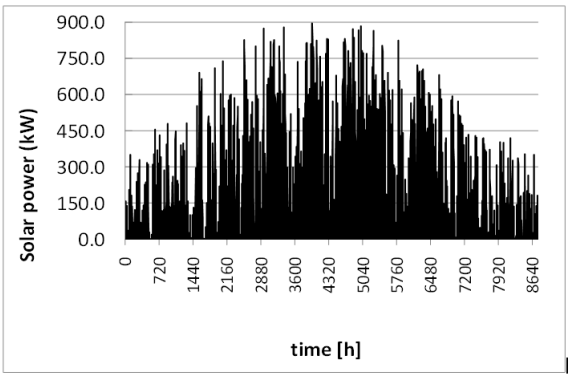

Fig. 4 Time variability of solar power in Lecce during 2007

As for the temperature of the thermal source (THS), it is considered variable in the range 65-115°C.
The design of the solar collector is not yet included in the procedure. To take into account the thermal losses, an overall efficiency of 80% is considered. This means that the rated power is multiplied by 0.8 to obtain the thermal power transferred to the working fluid (PHS).

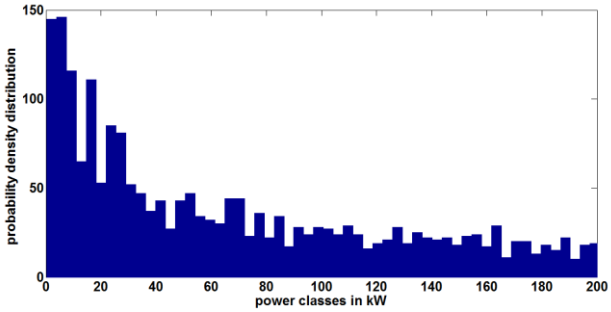

Fig. 5 Probability density distribution of solar power in Lecce during 2007

2.2 STEP B: List of fluids

Tchanche et al. [8] performed research in the area of working fluid selection for low temperature ORCs and listed 20 suitable fluids taking into account not only their thermodynamic properties but also safety and environmental issue. In the present investigation, three potential fluids were considered: R123, R245fa, R134a since they were available in the Refprop 8 database. Other fluids will be taken into account in the future use of the proposed methodology.

2.3 STEP C: Thermodynamic properties and flow rate

Mass and energy balance equations are written for all cycle components and for the overall cycle under the assumption of steady state operation.

Starting from power (P_{HS}) and the temperature (T_{HS}) of the thermal source defined at steps A and the organic fluid defined at Step B, this step only requires the discretionary over-heating to be defined and a pinch point analysis of the heat recovering vapor generator to calculate T_4.

Due to the concave shape of the vapor saturation curve of some organic fluid, the use of Over-Heating is not compulsory in ORC power plants. The Over Heating is design parameters that will be referred to as OH in the investigation. Its value allows the calculation of T_4 as the difference between T_{HS} and OH. Then, the evaporation pressure P_{evap} is automatically defined by the fluid and T_{evap}.

In the same way, starting from the temperature of the cooling medium, it is possible to define the condenser temperature T_{cond} an P_{cond} by assuming a reasonable value for the condenser pinch point.

At the end of the first three steps, the thermodynamic states 1, 4 and 6 are known. Thermodynamic state 2 can be easily calculated assuming that a isochoric process takes place in the pump from P_{cond} to P_{evap}. States 3, 4 and 5 depends on the values of the expander and regenerator efficiency that can be assumed from literature data. The values will be then corrected at the end of Step D.

For each thermodynamic state, a complete knowledge of the fluid properties is possible by linking the Matlab script used for the power plant model with the Refprop v. 8 database.

The knowledge of the enthalpy of fluid at state 3 and 4 allows the estimation of the flow rate by writing the energy balance of the vapor generator.

$$\dot{M} = \frac{0.8 \cdot \dot{Q}_{solar}}{h_4 - h_3} \quad (1)$$

Note that a constrain has been included in the present investigation to exclude configurations that require values of the volumetric flow rate higher that 12 liter per second (limit value for a Scroll expander).

2.4 STEP D: Model of the expander

The rotating speed of the expander is assumed to be linked with the grid frequency. Thus, the only way to change it is to increase the number of generator poles as in **Table 1**. Inefficiencies of the generator are neglected in the present investigation.

The second design parameter of the expander is the Built-In Volume Ratio (BVR) ([13,14]). Its choice will be performed in the optimization (step F).

A key point to be addressed is also the analysis of the behavior of the optimized power plant at off-design conditions by considering appropriate control stragegies , i.e. by regulating the BVR according to the actual temperature of the thermal source as suggested by M. Tahir et al. [15].

Table 1 Accepted speed value for the expander

Poles	*RPM & 50 Hz*
2	3,000
4	1,500
6	1,000
8	750
10	600
12	500
14	428.6
16	375

According to its BVR and the valus of vaporization and condensation pressures, the expander can operate in three different regimes:

- Under-expansion: the pressure reached by the fluid when the vane communicate with the discharge environment is higher than backpressure;
- Over-expansion: the pressure reached by the fluid when the vane communicate with the discharge environment is lower that backpressure;
- Design point;

The last regime is obtained when the pressure of the fluid at the end of the internal expansion produced by the BVR coincides with the condenser pressure. Being a special case of the first two modes of operation, it will not be analyzed in detail.

The expander is modeled as a sequence of simple thermodynamic processes in series and parallel (as suggested by [14]) to that take into account the thermal and fluid dynamics losses of the positive displacement machine.

The heat exchanges between the fluid and the walls are complex to model because of the variable temperature of the fluid and the difficulties in defining the exchange surface and the thermal convective and conductive coefficients. In the present investigation, the temperature of the wall is assumed constant and calculated as:

$$T_w = \frac{T_4 - T_{5,is}}{2} \quad (2)$$

Where $T_{5,is}$ is the hypothetical temperature that should be reached with a isentropic process.

The heat transfer is modeled through two isobaric processes. The first one is assumed to take place at the expander inlet where the fluid is hotter than the walls. The heat exchanged causes an increase of the fluid enthalpy from $h_{as,1}$=h4 to $h_{as,2}$:

$$\dot{Q}_{wall,1} = \dot{M}(h_{as,1} - h_{as,2}) = h_{as} S_1 \cdot (T_{as,1} - T_w) \quad (3)$$

The intensity of the heat transfer depends from the thermal coefficient and the exchange surface that are grouped in a single parameter to be tuned by comparison with experimental data. Since the model is used to design the size of the expander, it is necessary to scale this parameter with the machine displacement. To this, the correlation suggested by [15] has been considered:

$$h_{as} S_1 = k_{as} \cdot \left(\frac{V}{V_n} \right)^{0.8} \quad (4)$$

The nominal convective heat transfer coefficient k_{as} will be tuned by comparison with experimental data.

At the exit of the expander, another heat transfer process is assumed to take place between the colder fluid and the walls.

$$\dot{Q}_{wall,2} = \dot{M}(h_{esp,2} - h_{esp,1}) = h_{es} S_2 \cdot (T_{es,1} - T_w) \quad (5)$$

Again the process is simulated with a isobaric, the nominal heat transfer coefficient k_{es} is tuned and then scaled with the displacement to consider different sizes of the positive displacement expander.

$$h_{es} S_2 = k_{es} \cdot \left(\frac{V}{V_n} \right)^{0.8} \quad (6)$$

After the first isobaric heat transfer process, the fluid flow is separated in the main flow, which continues the evolution in the machine, and the leakage flow, which is laminated with an isenthalpic from evaporation to condensation pressure. The leakage flow rate is evaluated as:

$$\dot{M}_f = \xi \sqrt{p_{as,2} - p_{cond}} \quad (7)$$

Where ξ is a leakage coefficient that can be assumed to depend from the BVR. Tarique [14] suggests the values of **Table 2.**

Table 2 Correlation between the leakage coefficient and the BVR

BVR	ξ
2.9	5.67*10-6
3.3	7.60*10-6
3.5	7.23*10-6
5.4	2.63*10-6
6.1	3.98*10-6

After the first isobaric heat transfer process and the separation of the leakage flow, the remaining flow rate is assumed to expand with a isentropic from "*as,2*" to "*ad*" according to the Built-in Volumetric Ratio. The enthalpy of the fluid is then increased in a isochoric process from "*ad*" to "*aint*" to take into account fluid dynamic frictions. Again, friction is taken into account with a friction coefficient Π depending on the BVR:

$$\Pi = \frac{h_{\text{int}} - h_{ad}}{h_{as,2} - h_{ad}} \quad (8)$$

The values suggested in literature [15] are reported in **Table 3**.

Table 3 Correlation between Π and BVR

BVR	Π
2.9	0.38
3.3	0.49
3.5	0.61
5.4	0.72
6.1	0.71

At the end of the isochoric process that simulates frictions, the organic fluid has reached a pressure P_{int}. The thermodynamic status is labeled as "*aint*". According to the value of P_{int} and P_{cond}, it is possible to define three operating mode of the expander:

a) $P_{int} < P_{cond}$ (over-expanded)

b) $P_{int} < P_{cond}$ (under-expanded)

c) $P_{int} = P_{cond}$ (ideal case)

The adaptation to the condenser pressure is modeled with an isenthalpic process.

The thermodynamic processes that model the under-expanded machine from the initial state 4 are illustrated in Fig. **1** while the corresponding evolution in the thermodynamic chart is in **Fig.2**.

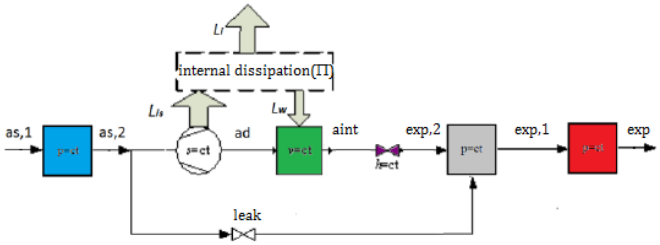

Fig. 1 Scheme of the thermodynamic processes considered in the case of under-expansion

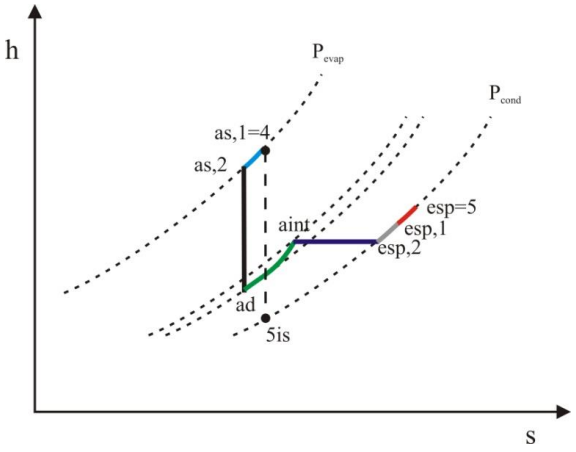

Fig.2 Representation in the enthalpy-entropy plane of the thermodynamic processes in under-expansion

Summing up, thermodynamic process in the under-expanded machine is described as:

- *as,1 – as,2*: first heat transfer process (organic fluid is cooled by heat transfer with the machine walls);
- The leakage flow (eq. 7) is separated and is laminated with an isenthalpic from P_{evap} to P_{cond};
- *as2 – ad*: the organic fluid is expanded with a isentropic from P_{evap} to P_{cond};
- *ad – aint*: friction causes the isochoric increase of fluid enthalpy defined by eq. 8;
- *aint – esp,2*, the organic fluid is laminated with a isenthalpic to reach the condenser pressure;
- *esp,2 – esp,1*: the leakage flow mixes adiabatically with the main flow;
- *esp,1 – esp*: second heat transfer process (organic fluid is heated by heat transfer with the machine walls).

The modeling of over-expansion is represented in **Fig. 3** and **Fig. 4**.

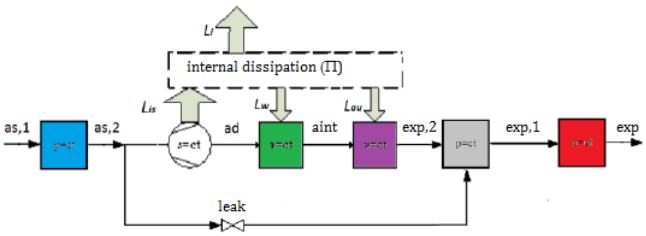

Fig. 3 Scheme of the thermodynamic processes considered in the case of over-expansion

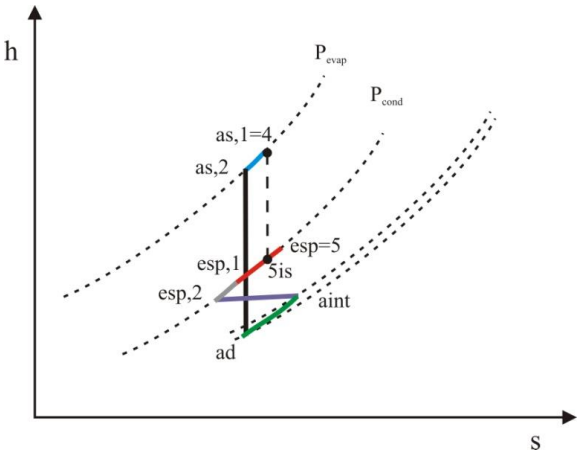

Fig. 4 Representation in the enthalpy-entropy plane of the thermodynamic processes in over-expansion

According to the nomenclature used in the figure, there is the following sequence of thermodynamic process:

Summing up, thermodynamic process in the under-expanded machine is described as:

- *as,1 – as,2*: first heat transfer process (organic fluid is cooled by heat transfer with the machine walls);
- The leakage flow (eq. 7) is separated and is laminated with an isenthalpic from P_{evap} to P_{cond};
- *as2 – ad*: the organic fluid is expanded with a isentropic from P_{evap} to P_{cond};
- *ad – aint*: friction causes the isochoric increase of fluid enthalpy defined by eq. 8;
- *aint – esp,2*, the organic fluid is compressed at constant enthalpy to reach the condenser pressure;
- *esp,2 – esp,1*: the leakage flow mixes adiabatically with the main flow;
- *esp,1 – esp*: second heat transfer process (organic fluid is heated by heat transfer with the machine walls).

Of course, in the case of design-point operation, P_{int} is equal to P_{cond} and *aint=asp,2*.

At the end of the elementary thermodynamic process, the final status of the fluid at the machine

outlet (state 5 of Figure 3) is calculated and temperatures T_5 and T_3 are upgraded repeating steps C-D until convergence is reached.

The internal power produced by the expanders can be calculated as:

$$P_{in} = \dot{M}(h_4 - h_5) + \dot{Q}_{wall,1} + \dot{Q}_{wall,2} \quad (9)$$

where $\dot{M}$ is the nominal flow rate of the power plant.

Mechanical frictions are calculated as:

$$P_w = \frac{2\pi}{60} n \cdot C_{w,n} \cdot V \quad (10)$$

Where the mechanical friction torque C_w is considered linearly dependent on the machine displacement (V) through the scaling parameter $C_{w,n}$ (friction torque per unit of displacement).

The power produced by the positive displacement expander can be calculated as:

$$P_{exp} = P_{in} - P_w \quad (11)$$

and mechanical efficiency as:

$$\eta_m = \frac{P_{in} - P_w}{P_{in}} \quad (12)$$

According to the elementary processes described above, it is possible to calculate the other efficiency of the machine like the volumetric efficiency:

$$\eta_v = \frac{\dot{M} - \dot{M}_f}{\dot{M}} = \frac{\dot{M}_{in}}{\dot{M}} \quad (13)$$

The thermodynamic processes that take place in an adiabatic machine can be compared with a isentropic process from inlet to outlet pressure by calculating the isentropic efficiency:

$$\eta_\vartheta = \frac{P_{in}}{\dot{M}(h_4 - h_{5is})} \quad (14)$$

where h_{5is} is the final enthalpy of the isentropic process (see Fig.2 and Fig. **4**).

The thermodynamic processes that take place in a machine without fluid dynamic friction can be compared with a isothermal process from inlet to outlet pressure by calculating the isothermal efficiency:

$$\eta_{isot} = \frac{P_{in}}{\dot{M} \cdot L_{isot}} \quad (15)$$

where L_{isot} is the internal work that can be obtained with the isothermal process from P_{evap} to P_{cond}.

In the present investigation, the positive displacement expander is neither adiabatic nor reversible. However, isentropic efficiency will be used as a measure of expander thermodynamic behavior. The overall efficiency of the expander is defined by multiplying the isentropic efficiency by mechanical and volumetric efficiencies.

The model of the positive displacement expander needs 4 parameters to be defined by comparison with experimental data: ξ, k_{as}, k_{es} and $C_{w,n}$.The tuning of the model has been performed with reference to the experimental data obtained by Tarique [14] with a Scroll expander with a displacement of 0.058 liter and a BVR equal to 3.5, using compressed air. Different tests were performed by changing temperature and pressure of the feeding air and measuring flow rate and net power (see **Table 4**).

Table 4 - Specification of the experimental test from [14]

test	*Pin[kPa]*	*Pus[kPa]*	*Tin[°C]*	*[ml/s]*
1	204.7	101.325	20	272
2	273.7	101.325	20	319
3	342.6	101.325	20	339
4	446.1	101.325	20	359
5	549.5	101.325	20	407
6	825.3	101.325	20	434
7	963.2	101.325	20	558
8	1135.3	101.325	20	608
9	1308.3	101.325	20	655

The best matching was found with the values of the parameters reported in **Table 5**. The results of the matching are shown in **Fig. 5**.

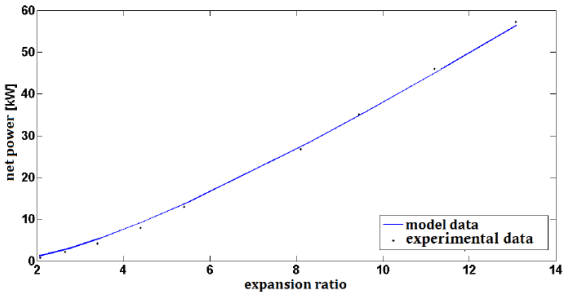

Fig. 5 Matching of the model with the experimental values of Tarique [14]

Table 5 Tuned values of the model parameters

Parameter	*Value*
ξ	2e-5 (m/kg)1/2
kas	0.001 W/°C
kes	0.01 W/°C
Cw,n	0.47 Nm

The model has been validated by comparison with the experimental data obtained by Lemort et al. [13] bon a Scroll expander (displacement 0.037 liter and

BVR 4.5) working with R123. The thermodynamic state of the fluid at the expander inlet and the operating conditions has been derived from the information reported in the paper.

The results obtained using the values of **Table 5** for the model parameters are reported in **Fig. 6**. The model predicts with reasonable accuracy the effect of changing speed and expansion ratio.

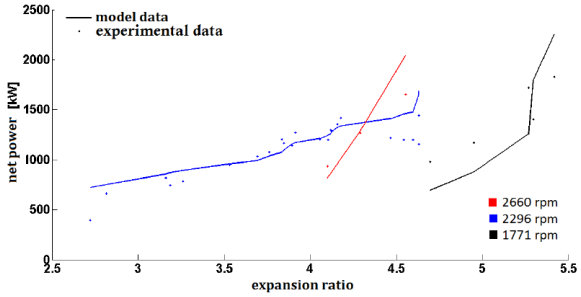

Fig. 6 Comparison with experimental data of Lemort et al. [13]

2.5 STEP E: Net power and efficiency

The net power produced by the power plant can be easily calculated as:

$$P_u = P_{\exp} - P_{pump} \tag{16}$$

Where the power absorbed by the pump is:

$$P_p = \frac{\dot{M} \cdot v_1 \cdot (p_{evap} - p_{cond})}{\eta_p} \tag{17}$$

The efficiency of the pump is considered constant and set equal to 0.8 regardless of operating conditions and fluid specification.

2.5 STEP F: Optimization by genetic algorithms

The choice of the design parameters of the power plant (**Table 6**) can be performed with a multi-objective genetic algorithm. In the present investigation, steps B – E have been implemented in a Matlab script included in the Modefrontier optimization environment [16]). Genetic Algorithms (GAs) have been chosen in this application for their robustness and their capability to deal with multi-objective optimizations. Furthermore, they are simple to use and to combine with existing simulation code without significant modifications and their efficiency is independent of the nature of the problem (in fact they have been used in previous investigation to optimize a variety of energy systems ([18],[21])

Table 6 List of design variable of the optimization

Variable	***Description***	*Range*	*Unit*
F.I.	Fluid index	1 ÷ 3 (R123; R245fa; R134a)	
R_on	Regenerator on\off	0 ÷ 1	
OH	Over-heating	0 ÷ 60	°C
THS	Temperature of the hot source	65-115	°C
BVR	Build-in volumetric ration	2.5 ÷ 5	
n	Expander speed	375 ÷ 3000	Rpm

The outputs of the Matlab script are used to set the optimization goals (Table 7).

Table 7 Goals of the optimization process

Description	*Goal*	
Net power of the power plant	P_u	To be maximized
Organic fluid flow rate	$\dot{M}$	To be minimized
Overall expander efficiency	$\eta_\theta \cdot \eta_m \cdot \eta_v$	To be maximized

3 Test case

The optimization has been performed with respect to a radiating power of 10 and 50 kW. For each case, an optimization run with a population of 100 individuals that evolves in 100 generations is considered.

A constrain has been added to avoid the choice of volumetric flow rate higher that 49 liter/s since the optimization was limited to the use of Scroll expander.

The results of the optimization for 10kW are represented in Fig. **7** as expander overall efficiency versus net power while Fig. **8** shows the corresponding results in terms of mass flow rate. Note that only the Pareto designs are shown. They are colored according to the working fluid: black for R123, red for R245fa and green for R134a. In each figure, the optimum point and the compromise design are shown. The meaning of the compromise design will be explained later. The optimum point was chosen so to have the maximum net power for each thermal power rating.

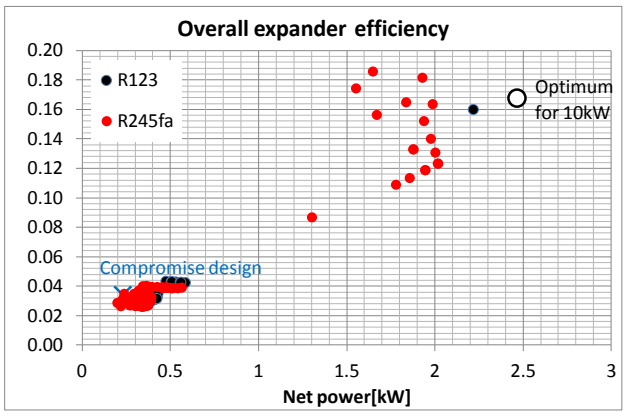

Fig. 7 Expander efficiency vs. net power (thermal power 10kW)

In the case of 10kW (Fig. **7** and Fig. **8**) fluid R123 gives the best results. In fact, this fluid guarantees higher expander efficiencies with the same flow rate while R245fa is better at 50kW (Fig. **9** and Fig. **10**). Note that R134a appears only once in the Pareto front in the case of 50kW thermal power.

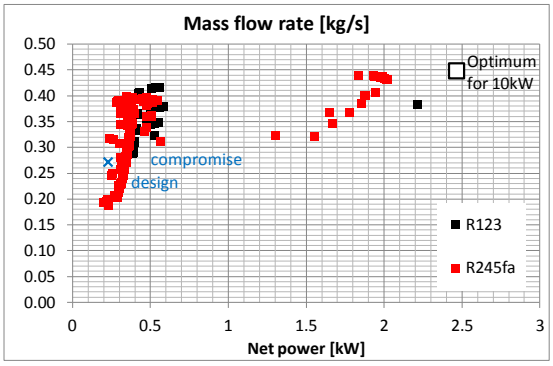

Fig. 8 Mass flow rate vs. net power (thermal power 10kW)

The specifications of the optimum points for the two values of thermal power are reported in **Table 8**.

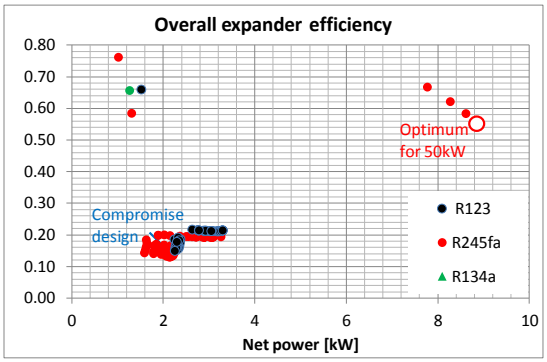

Fig. 9 Expander efficiency vs. net power (thermal power 50kW)

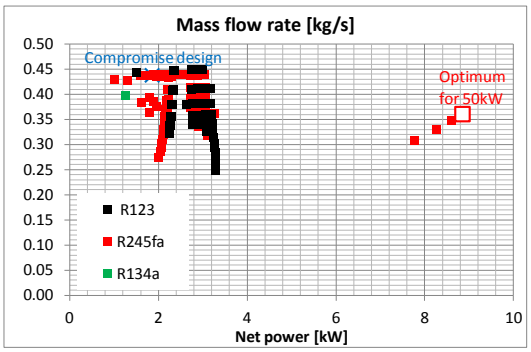

Fig. 10 Mass flow rate vs. net power (thermal power 50kW)

The expander optimized for 50kW presents a larger displacement (to dispose the greater flow rate) and a BVR slightly lower compared to the case with 10kW. For 10 kW the system reaches the overall efficiency of about 30% while only 18% is found in the case of 50kW. Better results could be obtained by considering a screw type expander (Fig. 2) that would allow the use of large flow rates.

Focusing on the case of 10kW, the optimal condition corresponds to an expander with overall efficiency of 44%. The transformations undergone by the fluid in the expander are illustrated in Fig. **11**. Note that the expander works nearly to ideal regime since the pressure defined by the BVR is almost coincident with the condenser pressure.

Table 8 Specification of the optimized power plants

Thermal POWER [kW]		***10***	***50***
	FLUID SELECTION	1, R123	2, R245fa
	regenerator	1	1
	OH [°C]	60	60
	Thermal source temperature [K]	361.4	374.4
INPUT	BVR	5	4.5
	n [rpm]	375	375
	P_u[kW]	2.47	7.489
	P_p[kW]	0.145	1.363
	Flow rate [kg/]	0.167	0.549
	Regenerating thermal power [kW]	34.22	129.1
	Condenser cooling power [kW]	30	111.9
	Power plant efficiency	0.29	0.18
OUTPUT	Expander efficiency	0.44	0.36
	P_{evap} [bar]	6	13
	T_3 [K]	421.5	434.4
	T_4 [K]	396.3	409.5
	Expander displacement [liters]	0.937	1.6

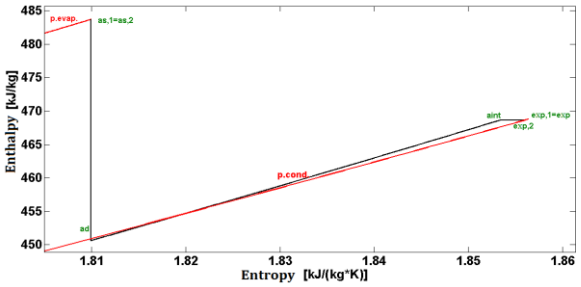

Fig. 11 Expander processes for the 10kW optimized powerplant

Fig. **12** shows the working cycle of the power plant with respect to the configuration optimized for 10kW.

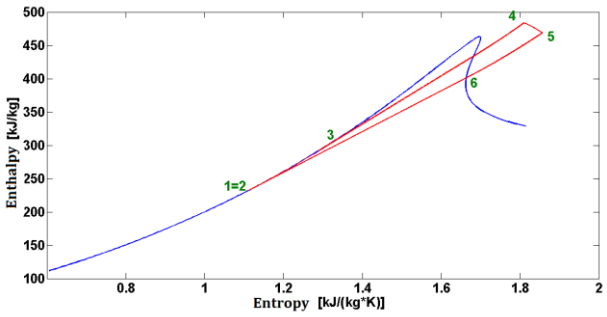

Fig. 12 Thermodynamic cycle for the 10kW optimized powerplant

Table 9 Specification of the compromise power plant

Thermal POWER [kW]		*10*	*50*
	FLUID SELECTION	2	
	regenerator ON	1	
	OH [°C]	60	45
INPUT	Vaporization temperature [K]	358.5	377.7
	BVR	4.5	
	n [rpm]	375	
	P_u[kW]	1.797	2.37
	P_p[kW]	0.205	0.522
	Flow rate [kg/]	0.128	0.191
	Regenerating thermal power [kW]	30.31	16.49
	Condenser cooling power [kW]	26.2	38.98
	Power plant efficiency	0.224	0.059
OUTPUT	Expander efficiency	0.434	0.337
	P_{evap} [bar]	9	14
	T_3 [K]	418.5	422.7
	T_4 [K]	396.7	396.1
	Expander displacement [liters]	0.49	

It is interesting to look for a configuration that would allow the use of the same fluid and of the same expander (displacement, BVR and speed of rotation) for both values of thermal power. This solution found is indicated with "compromise design" in the graphs showing the Pareto fronts of the optimization. The specification of this configuration is shown in Table 9. Note that the power plant efficiency is much lower than the optimized as expected in a power plant working with a large variability of thermal power.

4 Conclusion

A procedure for the design of a small solar-powered ORC plant employing a scroll-type expander has been implemented. The expander has been modeled as a sequence of elementary thermodynamic processes addressing thermal exchanges, fluid dynamic losses, leaks and losses of mechanical origin. The model has been tuned and validated by comparison with experimental data from literature to verify its predictive ability when varying the working fluid, the geometry of the machine, the speed of rotation and the expansion ratio.

The sizing procedure was applied to two values of the radiant thermal power (10 and 50kW) obtaining the optimum configuration for each power as well as a compromise solution that allows to operate the plant with both values of solar power using the same working fluid and the same volumetric expander.

Future developments of the procedure will relate to the possibility of taking into account other fluids, other types of expanders (expanders screw and radial turbines) and the executions of robust optimizations to obtain good efficiencies over a certain range of solar power.

References:

[1] D.L. Fenton, G. H. Abernathy, G. A. Krivokapich, J. V. Otts., Operation and Evaluation of the Willard Solar Thermal Power Irrigation System, Solar Energy, v. 32, no 6. 1984, pp. 735-751.

[2] Larson, Dennis L., Operational Evaluation of the Grid-Connected Coolidge Solar Thermal Electric Power Plant, Solar Energy, v. 38, no. 1, 1987, pp. 11-24.

[3] Cable, R. G.; Cohen, G. E.; Kearney, D. W.; Price, H. W., SEGS Plant Performance 1989-1997. Morehouse, J. M.; Hogan, R. E., eds. Solar Engineering 1998. Proceedings of the International Solar Energy Conference, 14-17 June 1998, Albuquerque, New Mexico (1998) pp.445-452 .

[4] B. F. Tchanche, G. Papadakis, G. Lambrinos and A. Frangoundakis, Fluid selection for a low- temperature solar organic Rankine Cycle, Applied Thermal Engineering Volume 29, Issues 11–12, 2009, pp. 2468–2476 6.

[5] E. W. Lemmon, M. L. Huber and M. O. McLinden, Reference fluid Thermodynamic and transport properties, NIST Standard Reference Database 23, 2007.

[6] X. D. Wang, L. Zhao, Analysis of zeotropic mixtures used in low-temperature solar Rankine cycles for power generation, Solar Energy, 83, 2009, pp. 605–13.

[7] G. Kosmadakis, D. Manolakos, S. Kyritsis, G. Papadakis, , Comparative thermodynamic study of refrigerants to select the best for use in the high- temperature stage of a two-stage organic Rankine cycle for RO desalination, Desalination, 243, 2009, pp. 74–94.

[8] B.F. Tchanche, G. Papadakis, G. Lambrinos, A. Frangoudakis, Fluid selection for a low-temperature solar organic Rankine cycle, Appl Therm Eng, 29, 2009, pp. 2468–76.

[9] J.L. Wolpert, S.B. Riffat, Solar-powered Rankine system for domestic applications, Appl Therm Eng, 16, 1996, pp. 281–289.

[10] A.M. Delgado-Torres, L. Garcia-Rodriguez, Analysis and optimization of the low-temperature solar organic Rankine cycle (ORC), Energy Conversion and Management 51, 2010, pp. 2846–2856.

[11] A.C. McMahan, Design & Optimization of Organic ORC Solar thermal powerplants, Master's thesis, University of Wisconsin-Madison, 2006,

[12] S. Quoilin, S. Declaye, Expansion Machine and Fluid Selection For The Organic Rankine Cycle, HEFAT2010, 7th International Conference on Heat Transfer, Fluid Mechanics

and Thermodynamics, 19-21 July 2010, Turkey, 2010.
[13] V. Lemort, S. Quoilin, C. Cuevas, Testing and modeling a scroll expander integrated into an Organic Rankine Cycle, Applied Thermal Engineering 29, 2009, pp. 3094–3102.
[14] Md. Ali Tarique, Experimental Investigation of Scroll Based Organic Rankine Systems, Master Thesis of Applied Science (MASc) University of Ontario Institute of Technology, 2011.
[15] M. B. M. Tahir, Characterictics of Small ORC System for Low Temperature Waste Heat Recovery, Journal of Environment and Engineering, Vol. 4 No. 2, 2009, pp. 375-385;
[16] S. Poles, E. Rigoni and T.Robic, MOGA-II Performance on Noisy Optimization Problems", Proceedings of BIOMA 2004, the International Conference on Bioinspired Optimization Methods and their Applications, 2004, pp. 51-62.
[17] TRNSYS, User manual TRNSYS 16, 2005
[18] T. Donateo, A. de Risi, D. Laforgia, On the Computer-Aided Conversion of a Diesel Engine to CNG-Dedicated or Dual Fuel Combustion Regime, Proceedings of the ASME 2012 Internal Combustion Engine Division Spring Technical Conference, May 6-9, 2012;
[19] T. Donateo, L. Serrao, G. Rizzoni, "A Two-step Optimization Method for the Preliminary Design of a Hybrid Electric Vehicle, International Journal of Electric and Hybrid Vehicles, Vol. 1, No. 2, 2008, pp. 142-165;
[20] T. Donateo, D. Pacella, D. Laforgia, A Method for the Prediction of Future Driving Conditions and for the Energy Management Optimization of a Hybrid Electric Vehicle, International Journal of Vehicle Design, Vol. 58, Nos. 2/3/4, 2012, pp. 111-133;
[21] T. Donateo, D. Pacella, D. Laforgia, Development of an Energy Management Strategy for Plug-in Series Hybrid Electric Vehicle Based on the Prediction of the Future Driving Cycles by ICT Technologies and Optimized Maps, SAE Paper 2011-01-0892, SP 2308 Advanced Hybrid Vehicle Powertrains, 2011